ARTICLE

# Argininosuccinate Lyase Deficiency Causes an Endothelial-Dependent Form of Hypertension

Jordan Kho,[1,2] Xiaoyu Tian,[3] Wing-Tak Wong,[4] Terry Bertin,[2] Ming-Ming Jiang,[2] Shan Chen,[2] Zixue Jin,[2] Oleg A. Shchelochkov,[2] Lindsay C. Burrage,[2] Anilkumar K. Reddy,[5] Hong Jiang,[6] Reem Abo-Zahrah,[7] Shuangtao Ma,[8] Ping Zhang,[9] Karl-Dimiter Bissig,[1,9] Jean J. Kim,[9] Sridevi Devaraj,[10] George G. Rodney,[7] Ayelet Erez,[2,11] Nathan S. Bryan,[2] Sandesh C.S. Nagamani,[2] and Brendan H. Lee[1,2,*]

Primary hypertension is a major risk factor for ischemic heart disease, stroke, and chronic kidney disease. Insights obtained from the study of rare Mendelian forms of hypertension have been invaluable in elucidating the mechanisms causing primary hypertension and development of antihypertensive therapies. Endothelial cells play a key role in the regulation of blood pressure; however, a Mendelian form of hypertension that is primarily due to endothelial dysfunction has not yet been described. Here, we show that the urea cycle disorder, argininosuccinate lyase deficiency (ASLD), can manifest as a Mendelian form of endothelial-dependent hypertension. Using data from a human clinical study, a mouse model with endothelial-specific deletion of *argininosuccinate lyase* (*Asl*), and *in vitro* studies in human aortic endothelial cells and induced pluripotent stem cell-derived endothelial cells from individuals with ASLD, we show that loss of ASL in endothelial cells leads to endothelial-dependent vascular dysfunction with reduced nitric oxide (NO) production, increased oxidative stress, and impaired angiogenesis. Our findings show that ASLD is a unique model for studying NO-dependent endothelial dysfunction in human hypertension.

## Introduction

Hypertension has estimated crude prevalence of 46% in the general adult population in the United States and is thus the most common risk factor associated with cardiovascular mortality.[1] Family and twin studies have demonstrated that blood pressure is clearly a quantitative genetic trait with high heritability estimated to be between 30% and 50%.[2] Although Mendelian forms of hypertension account for fewer than 1% of individuals with hypertension, study of these rare forms has provided significant insights into the complex pathogenic mechanisms causing primary hypertension. With the exception of mutations in *PDE3A*[3] (MIM: 123805) that causes hypertension and brachydactyly syndrome (MIM: 112410), all genes known to be associated Mendelian forms of hypertension encode components involved in the renal handling of volume and solutes or in the mineralocorticoid pathway.[4] Endothelial function is critical for the maintenance of normal blood pressure and endothelial dysfunction has been shown to be an important risk factor for development of hypertension.[5] Whereas preclinical models with endothelial dysfunction have been previously reported to develop hypertension, to the best of our knowledge, a Mendelian form of human hypertension that is primarily driven by endothelial dysfunction has not demonstrated to date. In this study, we show that the inborn error of metabolism, argininosuccinate lyase deficiency (ASLD), can manifest with endothelial-dependent hypertension.

ASLD (also known as argininosuccinic aciduria [MIM: 207900]) is the second most common urea cycle disorder (UCD). The urea cycle enzyme ASL catalyzes the cleavage of argininosuccinate into L-arginine and fumarate, the penultimate step in the generation of urea. In addition to the role in ureagenesis in the liver, ASL is also required in multiple tissues for the endogenous synthesis of L-arginine, a semi-essential amino acid that serves as a substrate for the synthesis of many important molecules including nitric oxide (NO). In fact, it is the sole enzyme in mammals through which *de novo* synthesis of arginine is accomplished. We have previously shown that ASL is critical for maintaining the stability of a NO-synthesis complex, which includes at minimum ASL, argininosuccinate synthase 1 (ASS1), nitric oxide synthase (NOS), the cationic arginine transporter (SLC7A1), and heat shock protein 90 (HSP90).[6] ASL is thus a key regulator of substrate availability for all NOS-dependent NO production, and not surprisingly, loss of ASL causes NO deficiency. NO regulates many pivotal pathways involved in the maintenance of normal vascular structure[7] and function.[8] We have previously reported that a mouse model global loss of ASLD develops systemic hypertension which is: (1) independent of the defect in hepatic ureagenesis, (2) secondary to NO deficiency, and (3) responsive to treatment with a

[1]Program in Developmental Biology, Baylor College of Medicine, Houston, TX 77030, USA; [2]Department of Molecular and Human Genetics, Baylor College of Medicine, Houston, TX 77030, USA; [3]School of Biomedical Sciences, the Chinese University of Hong Kong, Shatin, NT, Hong Kong; [4]School of Life Sciences, the Chinese University of Hong Kong, Hong Kong, Shatin, NT, Hong Kong; [5]Department of Medicine – Cardiovascular Sciences, Baylor College of Medicine, Houston, TX 77030, USA; [6]Brown Foundation Institute of Molecular Medicine, University of Texas Health Science Center, Houston, TX 77030, USA; [7]Department of Molecular Physiology and Biophysics, Baylor College of Medicine, Houston, TX 77030, USA; [8]Division of Nanomedicine and Molecular Intervention, Department of Medicine, Michigan State University, East Lansing, MI 48823, USA; [9]Center for Cell and Gene Therapy, Baylor College of Medicine, Houston, TX 77030, USA; [10]Department of Pathology and Immunology, Baylor College of Medicine, Houston, TX 77030, USA; [11]Department of Biological Regulation, Weizmann Institute of Science, Rehovot 76100, Israel
*Correspondence: blee@bcm.edu
https://doi.org/10.1016/j.ajhg.2018.07.008.

NOS-independent NO source, e.g., sodium nitrite.[6,9] Furthermore, by *in vitro* studies in fibroblasts and *in vivo* stable isotope studies, we have shown that humans with ASLD show evidence of NOS-dependent NO deficiency.[6,9] As ASLD is a human model of systemic NO deficiency, we investigated whether the human hypertension is primarily due to loss of cell-autonomous production of NO in endothelial cells and the consequence of ASL deficiency on vascular function and structure.

## Material and Methods

### Human Studies

Blood pressure measurements were recorded in a convenient sample of eight children with ASLD who were enrolled in a randomized clinical trial evaluating the effects of high dose versus low dose of arginine therapy on hepatic function tests (ClinVar: NCT00345605).[10] This was a single-center study conducted at Texas Children's Hospital and Baylor College of Medicine (BCM), Houston, TX, USA. The study protocol was approved by the NICHD and the Institutional Review Board of BCM. The study was monitored by a data safety monitoring board of the NICHD. Informed consent was obtained from all participants. Subjects with a confirmed diagnosis of ASLD, weight $>$ 10 kg, and serum creatinine less than 1.5 mg/dL were included in the study. During this study, individuals with ASLD were admitted at the Clinical Research Center of Texas Children's Hospital for a duration of 2 weeks. In this convenient cohort, blood pressure measurements were obtained every day by a trained nurse or medical assistant using an automated blood pressure apparatus. The blood pressure readings were converted into age-appropriate percentile values based on age, sex, and height and were compared to expected data in the control population.[11]

### Generation of Endothelial-Specific Conditional ASL Knockout Mice

$Asl^{flox[FRT\text{-}neo\text{-}FRT]/+}$ mice carrying the neomycin phosphotransferase (*neo*) gene were generated as previously described.[6] The $Asl^{flox[FRT\text{-}neo\text{-}FRT]/+}$ mice were crossed with transgenic mice expressing Flp recombinase to remove the *neo* cassette, leaving behind the loxP sites flanking exons 7–9 of *Asl*. The resulting mice with the $Asl^{flox/+}$ allele were interbred to generate $Asl^{flox/flox}$ mice. The $Asl^{flox/flox}$ mice were backcrossed onto the C57BL/6 background for at least five generations. These backcrossed $Asl^{flox/flox}$ were mated with transgenic mice bearing cre-recombinase expressed under the control of the cadherin5 promoter (B6.FVB-Tg(Cdh5-cre)7Mlia/J; Jackson Laboratory) to generate mice specifically lacking *Asl* in the endothelium: $Asl^{flox/flox}$, $Cdh5Cre^{tg/+}$, or *Asl* cKO. $Asl^{flox/flox}$ littermates were used as controls in all experiments. Only male mice were used for experimentation. The mice were maintained on a custom-formulated arginine-, nitrite-, and nitrate-free diet (Dyets Inc.) from week 4 until blood pressure measurements were obtained at 15 weeks of age. All studies were performed with approval from the Baylor College of Medicine Institutional Animal Care and Use Committee.

### Vascular Studies in Mice

For blood pressure measurements, mice were anesthetized with 1.5% isoflurane (in 100% oxygen) that was administered at a continuous flow rate of 20 mL/min (VetEquip). The neck and xiphoid areas were shaved, and the anesthetized mouse was placed in a supine position with its paws taped to electrodes on a temperature-controlled EKG board. The right carotid artery of the mouse was isolated and tied off distally, and the proximal end was temporarily occluded. A small cut was made in the artery, and a 1.0F (0.33 mm) Millar pressure catheter (Millar Instruments, SPR-100) was inserted and held in place with a suture loosely tied over the artery-catheter overlap region. The proximal end of the artery was then opened, and the catheter was advanced into the ascending aorta as close as possible to the aortic root. A second suture was tied over the artery-catheter overlap to prevent any blood leakage as the catheter was advanced. After allowing for a minute of stabilization, two 2-s segments of blood pressure along with EKG were captured and stored using the DSPW workstation (Indus Instruments) for offline analysis. The catheter was then advanced into the left ventricle (LV) of the mouse and again after a minute of stabilization, two 2-s segments of LV pressure along with ECG were captured and stored. Systolic, diastolic, and mean pressure were extracted from the stored aortic pressure files.

For aortic ring relaxation experiments, mice were anesthetized with isoflurane. A thoracotomy was performed to expose thoracic and abdominal aorta. A 25-gauge syringe was inserted into the apex of left ventricle and perfused free of blood with oxygenated Krebs Henseleit buffer. The right atrium was cut to provide an exit port for the blood. The aorta was removed and cleaned of all fat and adventitia. The aorta was cut into 2-mm-long segments and mounted on a four-channel wire myograph (AD Instruments). Vessel rings were maintained in 10 mL organ baths with oxygenated Krebs buffer (95% $O_2$ and 5% $CO_2$) at 37°C. Rings were allowed to equilibrate for 80 min with the buffer in each organ bath being changed every 20 min. One gram pretension was placed on each aortic ring (appropriate starting tension for optimal vasomotor function as determined in previous experiments). An eight-channel octal bridge (Powerlab) and data-acquisition software (Chart v.5.2.2) were used to record all force measurements. After equilibration for 80 min, 1 μM phenylephrine was added to each ring for submaximal contraction. After stabilization, increasing concentrations of acetylcholine were added to each bath to determine the endothelial-dependent relaxation which was expressed as percent reversal of phenylephrine-induced constriction.

### Endothelial Cell Culture and siRNA Experiments

HAECs (Lonza, CC-2535) were cultured in EGM2 BulletKit Medium (Lonza) and used before passage 9. To knock down *ASL* expression in HAECs, we used Silencer Select siRNAs obtained from ThermoFisher Scientific (s1669). siRNA transfection was performed in a 12-well or 6-well plate format using Lipofectamine RNAiMAX (ThermoFisher Scientific). For 12-well plate format, $6 \times 10^5$ cells of HAECs were plated on each well 1 day before transfection. We used 24 pmol siRNA and 4 μL Lipofectamine reagent per well. To assess knockdown efficiency, total RNA was collected 48 hr post-transfection. Non-targeting control siRNA (Dharmacon), referred to as siControl, was used as a control in all experiments.

### RNA Isolation and Real-Time qPCR

Total RNA was isolated from cells using TRIzol reagent (Invitrogen) and Direct-zol RNA MiniPrep (Zymo Research) with on-column DNase digestion. SuperScript III First-Strand Synthesis System (ThermoFisher Scientific) was used to synthesize first-strand cDNA from total RNA. qPCR was performed on the LightCycler

instruments (Roche) using SYBR Green I Master reagents (Roche) according to the manufacturer's recommendations. Relative mRNA expression was normalized to a reference gene (*β2-Microglobulin* or *GAPDH*).

### iPSC Generation, Culture, and Characterization

Primary skin fibroblasts from ASLD-affected subjects were provided by Baylor Genetics Laboratories. Fibroblasts were cultured in alpha MEM (Hyclone) with 10% FBS (Hyclone), 2 mMol/mL L-Glutamine (Hyclone), 50 U/mL penicillin, and 50 μg/mL streptomycin (Hyclone). The HSCC-003iPS (Ctrl 1) cell line was generated using dermal fibroblasts from a 22-year-old healthy male donor (ZenBio, lot # DFM062509),[12] Ctrl 2 cell line from a 61-year-old healthy male donor, and the HSCC-022iPS (Ctrl 4) cell line from a 16-year-old healthy male donor (CRL-2529, ATCC).

iPSC lines were generated from control and ASLD fibroblasts using two methods: by transduction with gamma-retroviruses encoding OCT4, SOX2, KLF4, and cMYC and by transduction with Sendai virus encoding OCT4, SOX2, KLF4, and cMYC (Table S2). Gamma-retrovirus reprogramming experiments were performed as previously described.[13] Sendai virus reprogramming experiments were conducted using CytoTune-iPS 2.0 Sendai Reprogramming Kit (ThermoFisher Scientific) per manufacturer's recommendations. Established iPSC lines were cultured and expanded in feeder-free TeSR-E8 medium (STEMCELL Technologies) on hESC-qualified Matrigel (Corning, 354277).

Chromosome G-banding analysis for karyotyping was performed by the T. C. Hsu Molecular Cytogenetics Facility, University of Texas MD Anderson (Houston, TX). STEMdiff Trilineage Differentiation Kit (STEMCELL Technologies) was used to differentiate established iPSC lines into three germ layers for assessment of pluripotency. Cells were harvested for gene expression analysis on day 5 for endoderm and mesoderm lineages and day 7 for the ectoderm lineage.

### Endothelial Differentiation and Characterization

iPSC were differentiated into endothelial lineage as previously described.[14,15] In brief, 70% confluent iPSCs were plated in an approximately 1:12 ratio and differentiation was induced 3 days after passaging using 6 μM CHIR99021 (Tocris), 40 ng/mL BMP4, and 20 ng/mL VEGF (Peprotech) in Advanced DMEM/F12 (ThermoFisher Scientific) for mesodermal induction for 2 days, followed by endothelial specification using 40 ng/mL VEGF, bFGF 10 ng/mL, and 10 μM SB431542 (Tocris) in Advanced DMEM/F12 for 5 days. On day 7, cells were dissociated with Accutase, washed, and incubated for 20 min at 4°C for subsequent FACS with the following antibodies: PE Mouse anti-Human CD144 (BD, 560410), Alexa Fluor 647 Mouse Anti-Human CD31 (BD, 561654), and/or PE Mouse Anti-Human CD309 (BD, 560872). Antibodies were diluted 1:100 in FACS buffer (5% FBS in 1× PBS). After sorting, iPSC-ECs were plated on fibronectin-coated surfaces for further expansion. iPSC-ECs were cultured up to passage 5 in EGM2 BulletKit Medium (Lonza).

To detect acetylated LDL uptake, iPSC-ECs were incubated with 7.5 μg/mL DiI-ac-LDL (Molecular Probes) for 6 hr at 37°C, washed, fixed with 4% paraformaldehyde (PFA, Sigma), and stained with DAPI (Molecular Probes) before imaging.

### Immunocytochemistry

To examine the expression of pluripotency or endothelial markers, cells were plated on chamber slides coated with Matrigel (for iPSC) or 2% gelatin solution (for endothelial cells). Cells were fixed with 4% PFA (Sigma) for 20 min at room temperature and washed 3 times with 1× PBS. To block non-specific antibody binding, cells were incubated in blocking buffer (3% donkey serum, 3% goat serum, 0.1% bovine serum albumin, and 0.2% Triton X-100 in PBS) for 1 hr at room temperature. Cells were then incubated overnight at 4°C in primary antibody diluted in blocking buffer solution. After overnight incubation, cells were washed 3 times and further incubated in diluted secondary antibodies (1:300, Alexa Fluor 488 or 594, Molecular Probes) for 1 hr at room temperature. ProLong Gold Antifade Reagent with DAPI (Molecular Probes) was used for mounting after the cells were washed three times with PBS.

For iPSC characterization, the following primary antibodies were used: anti-OCT4 (Stemgent, 09-0023), anti-TRA-1-81 (Stemgent, 09-0011), and anti-SOX2 (Abcam, ab97959). For endothelial cell characterization, the following primary antibodies were used: anti-CD31 (R&D Systems, BBA7), anti-CD144 (R&D Systems, AF938), anti-vWF (Abcam, ab6994), and anti-eNOS (BD, 610297).

### Nitric Oxide, ROS, and cGMP Measurement

NO relative concentration was quantified using DAF-FM Diacetate (ThermoFisher Scientific). Equal number of cells ($1 \times 10^5$) from each sample were incubated with 10 μM of DAF-FM Diacetate for 60 min at room temperature. Cells were then washed three times with 1× PBS before fluorescence signal was measured using fluorescent microplate reader.

ROS level was measured using DCFH-DA (ThermoFisher Scientific). Endothelial cells were seeded on a fibronectin-coated 96-well plate in EGM2 media at a concentration of $10^4$ cells per well. The cells were washed with 1× PBS three times and then incubated with DCFH-DA (10 μM) for 20 min at 37°C. The cells were then washed again with 1× PBS three times and the dye was allowed to de-esterify for 20 min at 37°C. DCF fluorescence was excited at 480 nm via a Sutter Lambda DG-5 ultra high-speed wavelength switcher. Emission intensity was collected at 510 nm at a rate of 0.1 Hz on a charge coupled device (CCD) camera (Photometrics, CoolSNAP MYO) attached to an Axio Observer (Zeiss) inverted microscope (40× $H_2O$ objective, 1.2 NA).

cGMP concentration was measured by competitive ELISA (Enzo). To collect cell lysates, we incubated $1 \times 10^5$ cells in 100 μL of 0.1 M HCl for 20 min at room temperature. All standards and samples were acetylated and assayed as per the instructions in the product's manual.

### Migration Assay

Wound healing assay was performed to assess cell migration. Endothelial cells were seeded on 12 well-plate ($6 \times 10^5$ cells/well) and cultured in EGM2 media until they reached confluence. A p1000 plastic pipette tip was used to create linear scratches on the cell monolayer. Media change was performed after "wounding" to remove cellular debris. Representative images are taken at specific scratched area using a phase-contrast microscope soon after media change and 8 hr after incubation at 37°C. Wound distances were calculated based on the average width of the scratched region.

### Angiogenesis Assay

For *in vitro* 2D Matrigel assay, HAECs or iPSC-ECs were plated on 24-well plates coated with Matrigel (Corning, 354234). A concentration of $5 \times 10^4$ cells per well were seeded in 0.5 mL of EGM2

media. Cells were incubated for 16 hr at 37°C before images were taken using phase-contrast microscope. Angiogenesis Analyzer plugin for ImageJ (Gilles Carpentier, Faculté des Sciences et Technologie, Université Paris Est, Creteil Val de Marne, France) was used to quantify tube formation.

*In vitro* 3D fibrin beads assay was performed as previously described.[16] In brief, 16 hr after siRNA transfection, HAECs were coated onto Cytodex 3 microcarrier beads (Amersham Biosciences) at a concentration of 400 cells per bead. After 3 hr of incubation at 37°C, coated beads were embedded in fibrin gel on 24-well plates. Human lung fibroblasts (Lonza, CC-2512) were then seeded on top of the fibrin gel at a concentration of $2 \times 10^4$ cells per well. Sprouting was quantified on day 7. Beads with at least 2 sprouts were randomly selected from each well and the number of sprouts were manually counted.

For *in vivo* Matrigel plug assay, iPSC-ECs were mixed with growth factor-reduced Matrigel (BD, 356231) at a concentration of $2 \times 10^6$ cells/mL. 200 μL of the cells-containing Matrigel solution were injected subcutaneously into the lower abdominal region of immunodeficient (NOD/SCID/IL2Rγ$^-$) mice (12 weeks old). 14 days after injection, plugs were collected, fixed in 4% PFA, and examined for human CD31 via immunostaining (Abcam, ab76533). Semiquantitative analysis of blood vessel-forming capacity was performed by counting the number of loops with positive CD31 staining using images of the entire plug.

### RNA-Seq

Total RNA was extracted from cells using AllPrep DNA/RNA/Protein Mini Kit (QIAGEN). cDNA libraries were generated by using KAPA Stranded mRNA-Seq Kit and KAPA Stranded RNA-Seq Kit with RiboErase (HMR) (Kapa Biosystems). Amplified cDNA was validated and quantified on Agilent Bioanalyzer with the High Sensitivity DNA chip. The purified libraries were normalized, pooled together, denatured, and diluted at final concentration of 1.8 pM. Furthermore, 1.3 mL of diluted pool was used to perform cluster generation, followed by 1 × 75 bp sequencing on NextSeq500 (Illumina). From each sample, we obtained about 35 million of reads. For gene expression analysis, reads were aligned to the reference genomes (hg38 UCSC assembly or mm10 UCSC assembly) using TopHat v2.0.14 and Bowtie v2.10 with following parameters (–no-coverage-search–library-type fr-firststrand –G were GFF file were obtained from Genome Reference Consortium Human Build 38 patch release 9 or Genome Reference Consortium Mouse Build 38 patch release 4). The distribution of alignments was analyzed using the Cufflinks v2.2.1, FPKM values were quantile normalized. Differential expression testing was performed using Cuffdiff v2.2.1. Pathways and upstream regulator analyses were performed by Ingenuity Pathway Analysis (IPA). Analysis was restricted to IPA database related to the vasculature, lung, and heart tissues.

### Statistical Analysis

Q-Q plots were generated to illustrate the deviation of observed values from the age- and sex-specific normal distribution using ggplot2 in R. The age- and sex-specific blood pressure data were generated using previously published.[11]

DCF fluorescent intensity was visualized by dot plot with ggplot2 in R. To convert continuous DCF fluorescent measurements to discrete variables, a bin size of 0.5 A.U. was chosen to generate a dot plot. To account for the correlation between iPSC lines generated from the same subject, mixed linear model was used to compare responses under different treatment conditions. The linear model was implemented with lmer function within lme4 R package. The model takes the measured responses as dependent variable, the treatment condition as independent variables. For modeling the random effect arising from variations across different individuals, the subject ID was used as the grouping factor in the lmer function. Because of the large sample size used for model fitting, a t-value cutoff as ±1.96 was used to determine significance of the independent variables.

## Results

### Blood Pressure Measurement in Humans with ASLD

First, we systematically assessed whether humans with ASLD have elevated blood pressures as this phenomenon has only been anecdotally reported.[9,17–19] We had previously conducted the largest randomized controlled trial in ASLD (ClinVar: NCT00345605) where 12 individuals with ASLD (8 children and 4 adults) were enrolled in a crossover trial to assess the effects of a high dose (500 mg/kg/day) versus a low dose (100 mg/kg/day) of L-arginine on hepatic function tests[10] (Table S1). The premise of this trial was to test whether increased argininosuccinate production by treatment of arginine contributed to chronic hepatic dysfunction observed in these individuals. During the study, systolic and diastolic blood pressures (SBP and DBP, respectively) were recorded over a 2-week inpatient hospitalization period by research staff. Because of the many environmental contributors to hypertension in adults, we limited our analyses of hypertension to children. Quantile-quantile (QQ) plots of SBP and DBP from the eight children (median age 12.1, range 9.1–13.8) demonstrated that the observed blood pressure values were significantly above the expected distribution from the normal population values[11] (Figure 1A). Furthermore, the blood pressures did not differ between the high-dose and low-dose arginine therapy arms (Figure 1B), suggesting that arginine supplementation could not correct the elevated blood pressure in this disorder, which is consistent with the structural requirement for ASL in all NOS-dependent NO production. These data suggest that children with ASLD are at increased risk for having elevated blood pressures and confirm the previous anecdotal reports in a controlled setting and demonstrate arginine resistance in this form of hypertension.

### Endothelial-Specific Asl Knockout

Regulation of blood pressure is a complex physiological system that involves multiple organs. To test whether the elevated blood pressure in ASLD was driven mainly by the loss of ASL in the endothelium, we generated an endothelial-specific knockout model of ASL (*Asl* cKO) by breeding a mouse model with a flox allele of *Asl*[20] with a transgenic model expressing cre recombinase expressed via the cadherin5 promoter. Both the *Asl* cKO and the control littermates ($Asl^{flox/flox}$) were maintained on a special diet that was free of nitrite, nitrate, and arginine to prevent

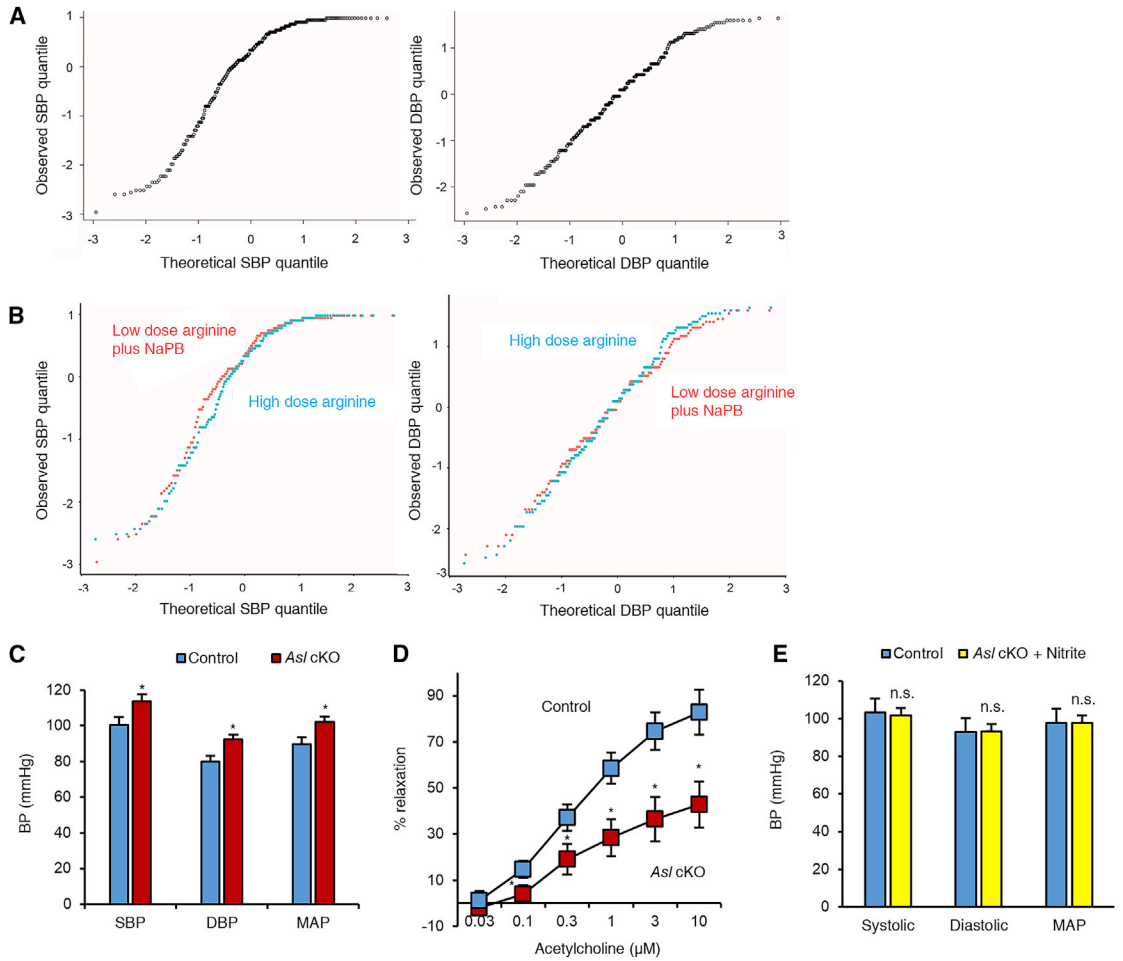


**Figure 1. Loss of ASL Is Associated with Elevated Blood Pressures**

(A) Quantile-quantile (QQ) plots of SBP and DBP in a convenient sample of eight children with ASLD who were enrolled in a randomized controlled trial evaluating the effects of low-dose arginine plus sodium phenylbutyrate (NaPB) versus high-dose arginine on hepatic functions (ClinVar: NCT00345605). The blood pressures in each treatment arm of the trial were collected at the clinical research center of Texas Children's Hospital over a 7–9 day period. The median number of blood pressure readings per subject was 35.5 (IQR, 30.75–40). Each dot in the scatterplot represents the intersection between an observed blood pressure quantile from one reading from one subject with an expected quantile from age- and sex-matched control population data. If the observed quantiles are similar to the normal population data, the points will lie on the 45° line on the scatterplot (i.e., x = y). However, the slope of the straight line of the plot is clearly greater than 45°, demonstrating left skewing of SBP and DBP readings. These show that the SBP and DBP in individuals with ASLD in this cohort were higher as compared to the age- and sex-matched data from the control population.

(B) The comparative QQ plots between the two treatment arms demonstrate that the elevated SBP and DBP are independent of the dose of arginine.

(C) Blood pressures measured using a carotid catheter in adult male mice demonstrate hypertension in *Asl* cKO mice as compared to their wild-type littermates (n = 9 control and n = 6 *Asl* cKO mice; mean [SD] age = 15.2 [0.6] weeks).

(D) Aortic ring relaxation, a classical *ex vivo* assay of endothelial-mediated NO signaling was significantly decreased in *Asl* cKO. The data represent mean percent relaxation from 4 segments from aorta of each mice (n = 3 *Asl* cKO mice and 5 control mice).

(E) Treatment of mice with sodium nitrite, a NOS-independent NO supplement, from 4 weeks of life prevents the development of hypertension in *Asl* cKO mice (n = 4 control and n = 4 nitrite-treated Asl cKO mice; mean [SD] age = 12.6 [0.3] weeks).

Bar graphs represent mean values while error bars represent the standard deviation. *$p < 0.05$; n.s., not significant; Student's t test (C, E), generalized linear modeling with dose of Ach, segment, and genotype as independent variables and percent relaxation as a dependent variable (D).

confounding of results due to dietary NO sources that may contribute to systemic NO via NOS-independent mechanisms. *Asl* cKO mice showed elevated SBP and DBP compared to their control littermates (Figure 1C). To demonstrate that the endothelial dysfunction was the primary driver of hypertension, we performed *ex vivo* aortic ring studies to assess endothelial-derived NO-mediated vascular relaxation. Preconstricted aortic rings from the *Asl* cKO mice showed impaired acetylcholine-induced endothelial-dependent relaxation (Figure 1D). *Asl* cKO mice also have normal serum level of alanine transaminase (ALT), aspartate aminotransferase (AST), lactate dehydrogenase (LDH), blood urea nitrogen (BUN), creatinine, albumin, and total protein, further suggesting that

hypertension was not secondary to liver or kidney dysfunction as may have been the case in the previously reported systemic deficiency model[6,9] (Figure S1). Importantly, treatment with sodium nitrite, a NOS-independent NO source, prevented the development of hypertension in *Asl* cKO (Figure 1E), supporting that systemic replacement was able to correct the cell-autonomous deficiency in endothelial cells. Overall, these results suggest that development of hypertension in ASLD is endothelial dependent and is driven, at least in part, by NO deficiency.

### siRNA-Mediated Knockdown of ASL in HAECs

To investigate the mechanisms by which ASL regulates vascular function, we knocked down *ASL* (MIM: 608310) in primary human aortic endothelial cells (HAECs) using siRNA (Figure 2A). Knockdown of *ASL* was associated with reduced intracellular levels of NO (Figure 2B) and decrease in NO signaling as evidenced by decreased intracellular cGMP (Figure 2C). As decrease in substrate availability for endothelial nitric oxide synthase (eNOS) has been shown to be associated with uncoupling of eNOS and increased generation of reactive oxygen species (ROS),[21] we measured ROS levels and found them to be significantly elevated with *ASL* knockdown (Figure 2D). Previous studies have demonstrated that NO is a key molecule regulating angiogenesis.[7] We thus investigated the effect of loss of ASL on cell migration and angiogenesis. HAECs knocked down for *ASL* showed impaired endothelial cell migration (Figure S2). Furthermore, HAECs with *ASL* knocked down demonstrated decreased formation of tube-like structures on Matrigel (Figures 2E and 2F) and impaired sprouting on 3D fibrin beads assay (Figure 2G). These *in vitro* assays show that loss of ASL in endothelial cells can result in alteration of both vascular function and structure.

### Modeling Vascular Dysfunction in ASLD with Human iPSC-Derived Endothelial Cells

Recent advances in induced pluripotent stem cell (iPSC) technology[13,22] have provided an innovative platform to model human diseases using iPSC-derived endothelial cells harboring mutations identified in affected individuals.[23–26] In order to develop an *in vitro* model to study hypertension in humans with ASLD, we generated iPSCs from two unrelated individuals with ASLD and hypertension. Reprogramming factors OCT4, SOX2, KLF4, and c-MYC were delivered via Sendai virus-mediated transduction to generate iPSCs from skin fibroblasts.[27] Two iPSC lines from each individual with ASLD and six lines from control subjects were obtained for further studies (Table S2). The pluripotency of iPSCs generated was confirmed based on expression of pluripotency markers and ability to differentiate into three germ layers (Figures S3A–S3C). All iPSCs had normal chromosome constitution (Figure S3D) and the ASLD iPSCs retained the same missense mutations as detected in the fibroblasts (Figure S3E). The control and ASLD iPSCs were differentiated into endothelial cells using standard protocols as previously published[14,15] and $CD31^+CD144^+$ cells were sorted by flow cytometry after 7 days of culture (Figure S4A). The sorted cells were confirmed to be endothelial cells based on expression of endothelial markers PECAM1, VE-Cadherin, eNOS, and von Willebrand factor (vWF) (Figure S4B). Furthermore, the iPSC-derived endothelial cells (iPSC-ECs) showed functional characteristics of mature endothelium as evidenced by the ability to form tube-like structures on Matrigel and uptake of acetylated low-density lipoprotein (LDL) (Figures 3E and S4C). Interestingly, we found that ASLD iPSCs differentiated less efficiently into endothelial cells than control iPSCs, as shown by reduced percentage of $CD31^+CD144^+$ and $Flk1^+$ population (Figure 3A). NO has been previously shown to drive endothelial differentiation of embryonic stem cells.[28,29] Thus, this result suggested that ASL-mediated NO production may be involved during vasculogenesis. Similar to the findings in HAECs knocked down for *ASL*, ASLD iPSC-ECs had reduced levels of intracellular NO and cGMP, increased ROS levels, and decreased angiogenic capacity as assessed by *in vitro* Matrigel assay (Figures 3B–3F). To assess the relevance of these findings *in vivo*, we performed Matrigel plug assay by mixing iPSC-ECs with Matrigel and injecting them into immunodeficient (NOD/SCID/IL2R$\gamma^-$) mice. ASLD iPSC-ECs showed reduced capacity to form blood capillaries and arterioles *in vivo* (Figure 3G).

### RNA-Sequencing Analysis in ASL-Deficient HAECs

To identify candidate downstream pathways dysregulated by endothelial NO and ASL deficiency, we performed RNA sequencing on RNA isolated from siControl and siASL-transfected HAECs. Gene expression profiling revealed that 6,795 genes were significantly dysregulated in ASL-deficient HAECs (Figures 4A and 4B). The expression pattern of top dysregulated genes was confirmed by qRT-PCR (Table S3, Figure S5). We also assessed the mRNA expression of the components of NO synthesis complex in ASL-deficient HAECs. We found that expression of all three NOS isoforms (*nNOS*, *iNOS*, and *eNOS*) remained unchanged. *ASS1* and *HSP90AA* mRNA expression was significantly upregulated while *SLC7A1* mRNA expression was significantly downregulated (Table S4, Figure S5). Using Ingenuity Pathway Analysis (IPA), we discovered that vasculature development, angiogenesis, vasculogenesis, and cell migration were the top dysregulated cellular functions, which is consistent with the phenotypes observed in ASL-deficient HAECs (Figure 4C). Among the top dysregulated canonical pathways were signaling pathways that have been previously associated with hypertension (aryl hydrocarbon receptor[30] and glucocorticoid receptor[31,32]) and angiogenesis (protein kinase A,[33] HGF/hepatocyte growth factor,[34] and PTEN[35]). Furthermore, IPA upstream regulator analysis revealed that a few members of TGFβ superfamily (TGFB1, ACVRL1/ALK1, and BMP6) and AGT, a precursor of angiotensin II, were predicted to be activated in

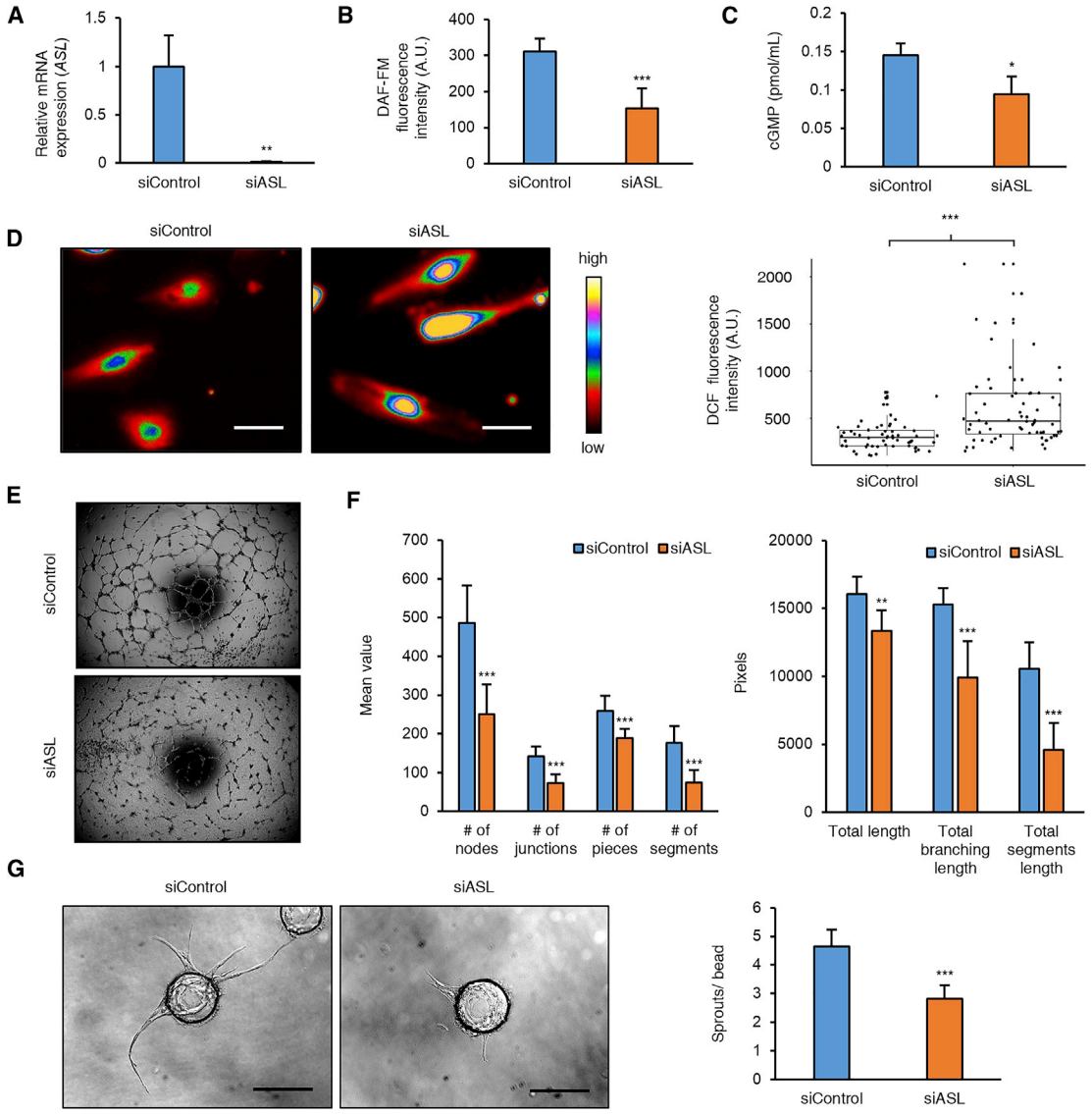


**Figure 2. *ASL* Knockdown in HAECs Leads to Decreased NO Signaling, Increased Oxidative Stress, and Impaired Angiogenesis**

(A) Relative mRNA expression in cultured HAECs 2 days after transfection with siASL and siControl (n = 3 biological replicates of siControl and siASL).

(B) Intracellular NO levels as measured by DAF-FM diacetate fluorescence assay (averaged from seven biological replicates with siControl and siASL).

(C) Intracellular cGMP levels show decreased NO signaling in cells transfected with siASL as compared to siControl (n = 3 biological for replicates siASL and siControl).

(D) Relative ROS levels as measured by DCF fluorescence assay (n = 59 cells siControl and 68 cells siASL). Boxplots represent median and interquartile values and whiskers represent outlier value within 1.5 times the interquartile range of quartiles. Shown are the representative images of siRNA-transfected HAECs after incubation with DCFH-DA. Scale bar, 25 μm.

(E) *In vitro* Matrigel angiogenesis assay shows decreased angiogenesis in ASL-deficient HAECs. HAECs were plated on Matrigel 1 day after siRNA transfection. Images were taken 16 hr after plating.

(F) Quantitative measurement of tube formation using Angiogenesis Analyzer tool from ImageJ (n = 7 siControl and 8 siASL).

(G) Fibrin gel sprouting angiogenesis assay was performed 24 hr after siRNA transfection wherein HAECs were coated onto beads and embedded in a fibrin gel seeded with human lung fibroblasts. Images were obtained 7 days after embedding and the average number of sprouts per bead in each well was quantified (n = 11 wells for siControl and 11 wells for siASL). Scale bar, 200 μm.

Bar graphs represent mean values while error bars represent the standard deviation. *$p < 0.05$, **$p < 0.01$, and ***$p < 0.001$. Student's t test or Mann-U-Whitney test were performed after checking for normality of the data.

ASL-deficient HAECs (Figure 4D). Activation of TGFβ and angiotensin II signaling pathways have been previously associated with endothelial dysfunction and hypertension.[36,37] Interestingly, a few regulators with known functions in endothelial activation (IKBKB, RELA, and IL17A) and ERG, an ETS transcription factor that has been shown to promote angiogenesis and vascular stability,[38] were predicted to be inhibited (Figure 4D). This molecular signature supports our discovery that ASL deficiency causes a dysregulation of vascular function and structure.

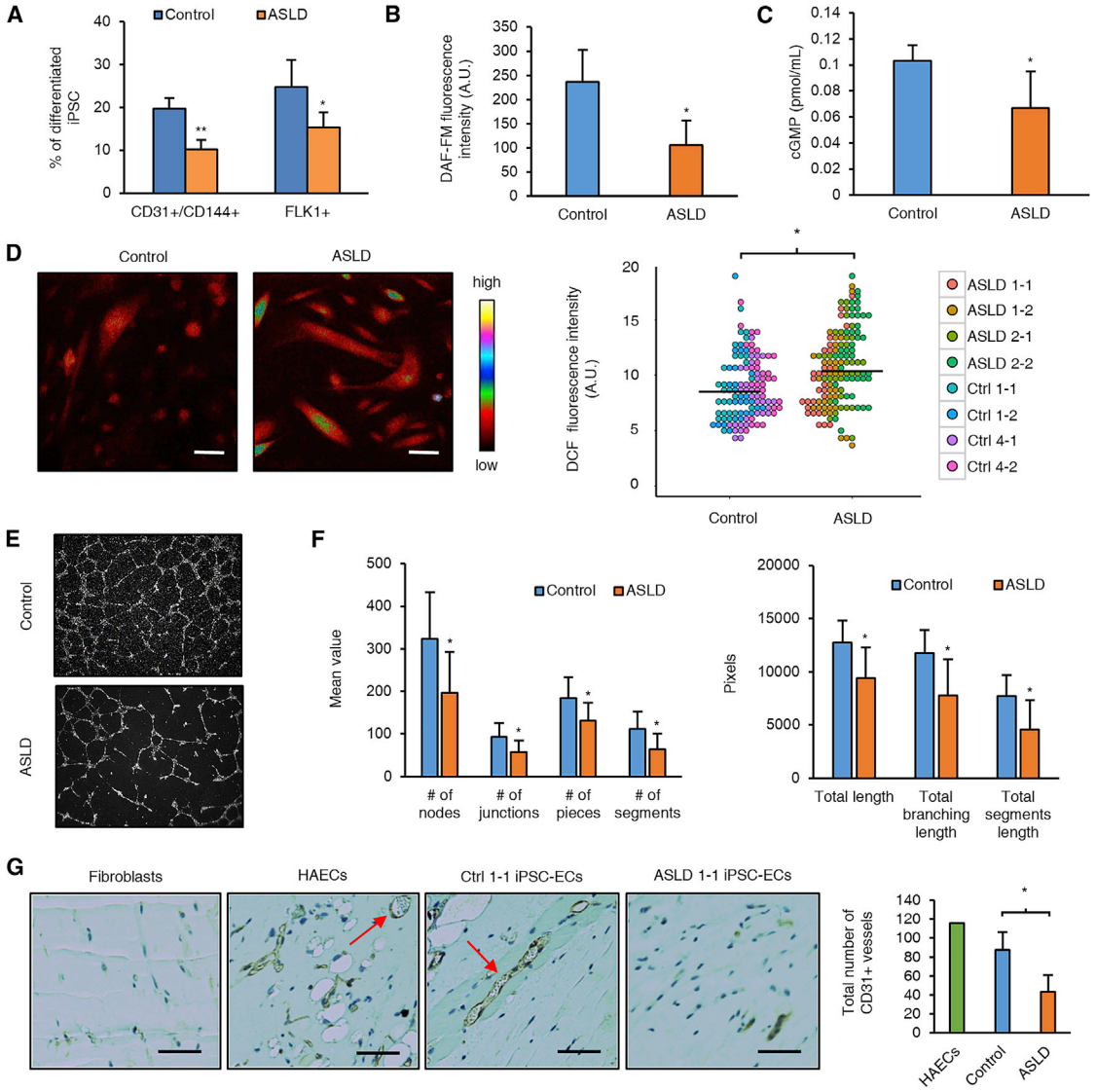


**Figure 3. iPSC-ECs from Individuals with ASLD Demonstrate Decreased NO Signaling, Increased Oxidative Stress, and Impaired Angiogenesis**

(A) Endothelial differentiation efficiency as shown by the percentage of $CD31^+CD144^+$ and $Flk1^+$ cells (n = 4 control iPSC-ECs and 4 ASLD iPSC-ECs).

(B) Measurement of intracellular NO levels in iPSC-ECs using DAF-FM diacetate fluorescence assay (n = 4 control iPSC-ECs and 4 ASLD iPSC-ECs).

(C) NO signaling as measured by intracellular cGMP levels are decreased in ASLD iPSC-ECs (n = 4 control iPSC-ECs and 4 ASLD iPSC-ECs).

(D) Relative ROS levels in iPSC-ECs as measured by DCF fluorescence assay (n = 122 cells from 4 control lines and 138 cells from 4 ASLD lines). Scale bar, 25 μm.

(E and F) Representative images and quantification of network formation obtained from *in vitro* Matrigel angiogenesis assay performed on iPSC-ECs (n = 3 control iPSC-ECs and 4 ASLD iPSC-ECs).

(G) *In vivo* Matrigel plug assay. iPSC-ECs were mixed with Matrigel and injected into immunodeficient (NOD/SCID/IL2R$\gamma^-$) mice. Human fibroblasts and HAECs were used as negative and positive controls, respectively. Representative images of fixed section of Matrigel plug collected 14 days after injection are shown. Blood capillaries (shown by red arrows) were stained with CD31 antibody. Formation of blood capillaries and arterioles was quantified by manually counting the number of $CD31^+$ loops in the entire plug (n = 3 control iPSC-ECs and 3 ASLD iPSC-ECs). Scale bar, 50 μm.

Bar graphs represent mean values while error bars represent the standard deviation. *$p < 0.05$. Intergroup differences based on genotype (i.e., control versus ASLD) was performed using a linear mixed model that accounted for the correlation between data obtained from the same iPSC clone of the same subject.

## Discussion

Using data from a human clinical trial, a conditional knockout model with ASL deficiency in the endothelium, and *in vitro* studies in HAECs and iPSC-ECs, we show that endothelial dysfunction is a primary driver of hypertension in ASLD. We propose that ASL deficiency in endothelial cells causes hypertension through at least two possible

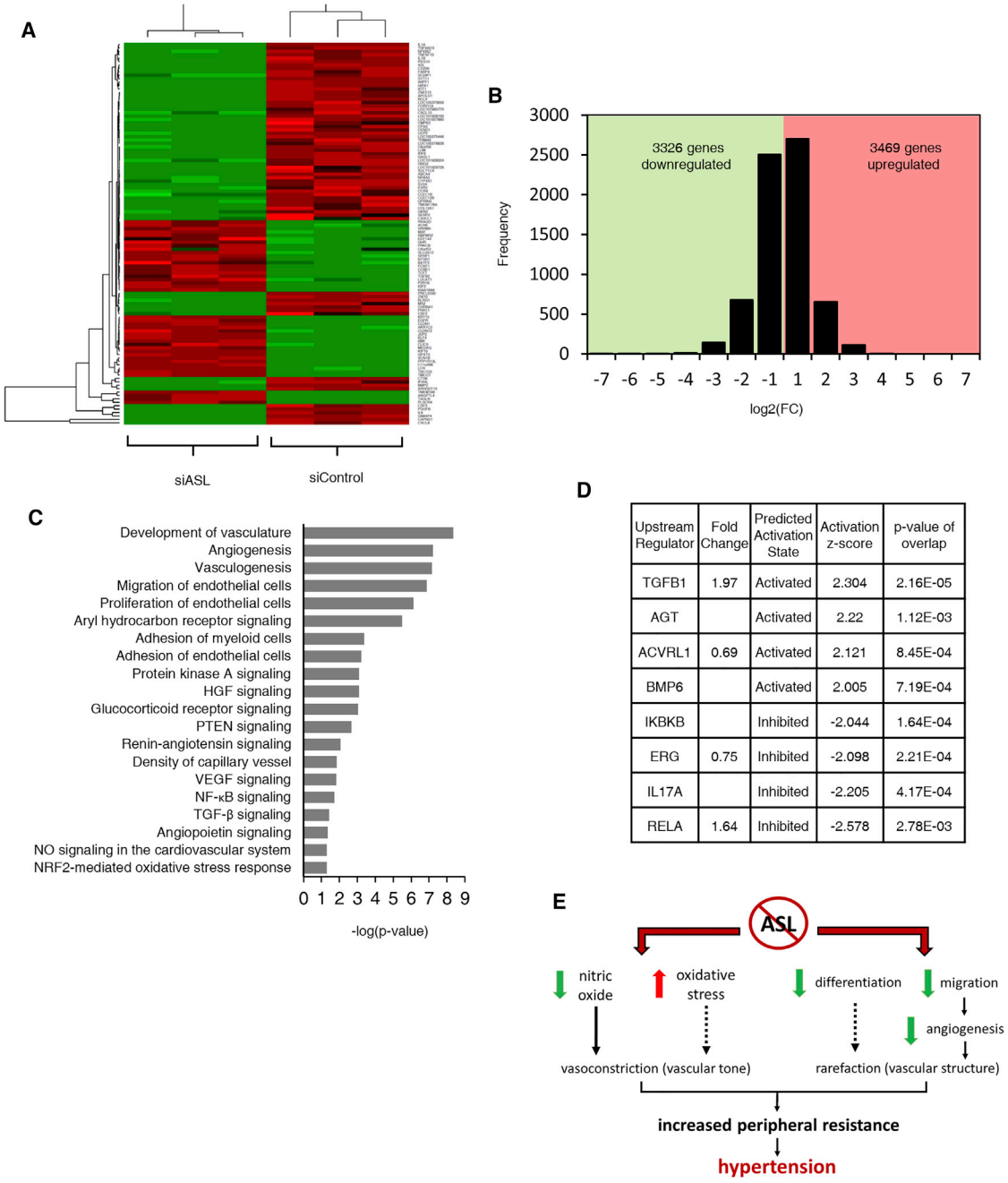


| Upstream Regulator | Fold Change | Predicted Activation State | Activation z-score | p-value of overlap |
|---|---|---|---|---|
| TGFB1 | 1.97 | Activated | 2.304 | 2.16E-05 |
| AGT | | Activated | 2.22 | 1.12E-03 |
| ACVRL1 | 0.69 | Activated | 2.121 | 8.45E-04 |
| BMP6 | | Activated | 2.005 | 7.19E-04 |
| IKBKB | | Inhibited | -2.044 | 1.64E-04 |
| ERG | 0.75 | Inhibited | -2.098 | 2.21E-04 |
| IL17A | | Inhibited | -2.205 | 4.17E-04 |
| RELA | 1.64 | Inhibited | -2.578 | 2.78E-03 |

**Figure 4. Loss of ASL Leads to Dysregulation of Transcriptome in Human Endothelial Cells**
(A) Heatmap showing hierarchical clustering of the top dysregulated genes in siASL-transfected HAECs.
(B) Histogram of genes that are differentially expressed in siControl- versus siASL-transfected HAECs.
(C) IPA analysis of top dysregulated pathways in ASL-deficient HAECs.
(D) IPA upstream regulator analysis showing genes predicted to be activated or inhibited in ASL-deficient HAECs based on the calculation of the activation Z-score.
(E) Working model of how ASL deficiency in endothelial cells leads to the development of hypertension.

mechanisms: increased vascular tone and altered vascular structure (Figure 4E). These data support that loss of ASL is associated with vascular tone and this may be mediated in part via (1) decreased production of endothelial NO, a potent vasodilator, and (2) increased vascular oxidative stress, which has been previously associated with high blood pressures in individuals with essential hypertension.[39] Whether oxidative stress directly alters vascular tone remains inconclusive. However, recent studies seem to support the hypothesis that vascular oxidative stress plays a causal role in the pathogenesis of hypertension.[40] ASLD may also promote hypertension by altering the overall vascular structure. Microvascular rarefaction, a phenomenon characterized by a loss of arterioles and

capillaries, is a hallmark of hypertension. This alteration of vascular structure is mainly caused by impaired angiogenesis. While the cause-effect relationship between hypertension and rarefaction remains inconclusive, some evidence suggests that rarefaction has a causal effect on the development. Impaired microvascular rarefaction was associated with predisposition to essential hypertension in young adult males.[41] Furthermore, recent studies from cancer clinical trials showed that there is a dose-dependent increase in risk of hypertension in individuals with cancer treated with anti-angiogenic agents.[42]

Our RNA-sequencing analysis in ASL-deficient HAECs not only is consistent with the phenotypes that we observed in our *in vitro* studies but also provides insights into pathways dysregulated in ASLD. Among the top dysregulated canonical pathways, we identified two that have been previously shown to regulate blood pressure in mouse studies: aryl hydrocarbon receptor and glucocorticoid receptor signaling pathways. Aryl hydrocarbon receptor is a ligand-activated transcription factor that is highly expressed in endothelial cells. Global and endothelial-specific knockout of aryl hydrocarbon receptor induces alteration in blood pressure.[30,43] Similarly, excess glucocorticoid has also been known to induce hypertension. Glucocorticoid exerts its effects via a wide variety of tissues, including endothelial cells.[32] Mice with endothelial-specific knockout of glucocorticoid receptor have been shown to be completely resistant to glucocorticoid-induced hypertension.[31] These data suggest that these pathways may share common components in the dysregulation of NO signaling and ASL deficiency.

In this study, we also present the use of iPSC-ECs as an approach for studying an endothelial-based form of Mendelian hypertension and further highlight its value for modeling other vascular diseases and specifically those caused by Mendelian mutations. Currently, this is one of the few that model an endothelial-dependent form of hypertension. One limitation of our iPSC model is the genetic heterogeneity that may exist among iPSC lines derived from multiple subjects though the effect size and comparison of multiple control and patient-derived iPSCs and use of isogenic HAECs supports the robustness of the findings. Still, generation of isogenic iPSC lines will provide a better model to study the function of ASL in future studies on downstream mechanisms. Individuals with ASLD typically harbor compound heterozygous mutations that may differentially affect enzyme activity and protein stability. This might explain why the siRNA-mediated knockdown model showed a more severe phenotype as compared to the iPSC model as they are closer to the null state.

Our findings have the potential to have translational significance not only for the treatment of individuals with ASLD but also in exploring the role of ASL and NO deficiency in primary hypertension. The immediate impact would be in clinical evaluation and management of individuals with ASLD. With the implementation of newborn screening across all 50 states in the United States, increased awareness of these rare disorders, and availability of treatment modalities that help dispose of waste nitrogen, the average lifespan of individuals with UCD has increased significantly.[44] Prevention of long-term complications such as hypertension could thus be of value in the management of individuals with ASLD. One obvious therapeutic option would be to use NOS-independent NO supplements. We are currently conducting a randomized, double-blind, placebo-controlled clinical trial (ClinicalTrials.gov: NCT02252770) to investigate whether this approach can be used to treat endothelial dysfunction in ASLD. Our results could also help foster studies that would evaluate rarefaction, aortic impedance, and pulse wave velocities in ASLD. In a broader context, our approach may be relevant to study not only endothelial-mediated hypertension but also NO signaling in the vasculature. The manipulation of the ASL-NOS system may also be a potential therapeutic target in primary, resistant forms of hypertension.

## Accession Numbers

The raw RNA-seq data have been deposited in the National Center for Biotechnology Information Sequence Read Archive (SRA) database under the accession code SRP152883.

## Supplemental Data

Supplemental Data include five figures and four tables and can be found with this article online at https://doi.org/10.1016/j.ajhg.2018.07.008.

## Acknowledgments

We are grateful to all individuals with ASLD who participated in the study. We thank Yuqing Chen and Sherry Li for assistance with mouse colony maintenance, Dr. Muralidhar Premkumar for help with *in vivo* mouse studies, Dr. Matthew Grol for help with Matrigel plug assay, and B.H.L. lab members for their technical assistance and suggestions. DNA Link assisted with RNA-seq and its analysis. This work was supported by the Clinical Translational Core of BCM Intellectual and Developmental Disabilities Research Center (HD024064, HD083092) from the Eunice Kennedy Shriver National Institute of Child Health and Human Development, the BCM Advanced Technology Cores with funding from the NIH (AI036211, CA125123, and RR024574), T32 GM007526 (B.H.L., A.E.), DK102641 (B.H.L.), AR061370 (G.G.R.), R56DK115461 (K.D.B.), R01HL134510 (K.D.B.), K08DK106453 (L.C.B.), and the National Urea Cycle Disorders Foundation. The clinical trial was supported by the Urea Cycle Disorders Consortium (UCDC) (U54HD061221). UCDC is a part of Rare Disease Clinical Research Network (RDCRN), an initiative of the Office of Rare Disease Research (ORDR), NCATS. This consortium is funded through collaboration between NCATS (U54HD061221) and the Eunice Kennedy Shriver National Institute of Child Health and Human Development (HD024064, HD083092, and U54HD061221) or the NIH. The content is solely the responsibility of the authors and does not necessarily represent the official views of the USDA, the Eunice Kennedy Shriver National Institute of Child Health and Human Development, or the NIH. S.S.N. was also

supported by the CSDA from the Doris Duke Charitable Foundation (2013095). The funds from the CSDA were not used for any animal-related research.

## Declaration of Interests

The authors declare no competing interests.

Received: March 15, 2018
Accepted: July 12, 2018
Published: August 2, 2018

## Web Resources

Clinical Trial, https://clinicaltrials.gov/
IPA, https://www.ingenuity.com
NCBI SRA, https://www.ncbi.nlm.nih.gov/sra
OMIM, https://www.omim.org/

## References

1. Muntner, P., Carey, R.M., Gidding, S., Jones, D.W., Taler, S.J., Wright, J.T., Jr., and Whelton, P.K. (2018). Potential U.S. population impact of the 2017 American College of Cardiology/American Heart Association High Blood Pressure Guideline. J. Am. Coll. Cardiol *71*, 109–118.
2. Miall, W.E., and Oldham, P.D. (1963). The hereditary factor in arterial blood-pressure. BMJ *1*, 75–80.
3. Maass, P.G., Aydin, A., Luft, F.C., Schächterle, C., Weise, A., Stricker, S., Lindschau, C., Vaegler, M., Qadri, F., Toka, H.R., et al. (2015). PDE3A mutations cause autosomal dominant hypertension with brachydactyly. Nat. Genet. *47*, 647–653.
4. Padmanabhan, S., Caulfield, M., and Dominiczak, A.F. (2015). Genetic and molecular aspects of hypertension. Circ. Res. *116*, 937–959.
5. Mordi, I., Mordi, N., Delles, C., and Tzemos, N. (2016). Endothelial dysfunction in human essential hypertension. J. Hypertens. *34*, 1464–1472.
6. Erez, A., Nagamani, S.C., Shchelochkov, O.A., Premkumar, M.H., Campeau, P.M., Chen, Y., Garg, H.K., Li, L., Mian, A., Bertin, T.K., et al. (2011). Requirement of argininosuccinate lyase for systemic nitric oxide production. Nat. Med. *17*, 1619–1626.
7. Cooke, J.P., and Losordo, D.W. (2002). Nitric oxide and angiogenesis. Circulation *105*, 2133–2135.
8. Tousoulis, D., Kampoli, A.M., Tentolouris, C., Papageorgiou, N., and Stefanadis, C. (2012). The role of nitric oxide on endothelial function. Curr. Vasc. Pharmacol. *10*, 4–18.
9. Nagamani, S.C., Campeau, P.M., Shchelochkov, O.A., Premkumar, M.H., Guse, K., Brunetti-Pierri, N., Chen, Y., Sun, Q., Tang, Y., Palmer, D., et al. (2012). Nitric-oxide supplementation for treatment of long-term complications in argininosuccinic aciduria. Am. J. Hum. Genet. *90*, 836–846.
10. Nagamani, S.C., Shchelochkov, O.A., Mullins, M.A., Carter, S., Lanpher, B.C., Sun, Q., Kleppe, S., Erez, A., O'Brian Smith, E., Marini, J.C., Lee, B.; and Members of the Urea Cycle Disorders Consortium (2012). A randomized controlled trial to evaluate the effects of high-dose versus low-dose of arginine therapy on hepatic function tests in argininosuccinic aciduria. Mol. Genet. Metab. *107*, 315–321.
11. National High Blood Pressure Education Program Working Group on High Blood Pressure in Children and Adolescents (2004). The fourth report on the diagnosis, evaluation, and treatment of high blood pressure in children and adolescents. Pediatrics *114* (2, Suppl 4th Report), 555–576.
12. Liu, R., Lee, J., Kim, B.S., Wang, Q., Buxton, S.K., Balasubramanyam, N., Kim, J.J., Dong, J., Zhang, A., Li, S., et al. (2017). Tead1 is required for maintaining adult cardiomyocyte function, and its loss results in lethal dilated cardiomyopathy. JCI Insight *2*.
13. Takahashi, K., Tanabe, K., Ohnuki, M., Narita, M., Ichisaka, T., Tomoda, K., and Yamanaka, S. (2007). Induction of pluripotent stem cells from adult human fibroblasts by defined factors. Cell *131*, 861–872.
14. Orlova, V.V., van den Hil, F.E., Petrus-Reurer, S., Drabsch, Y., Ten Dijke, P., and Mummery, C.L. (2014). Generation, expansion and functional analysis of endothelial cells and pericytes derived from human pluripotent stem cells. Nat. Protoc. *9*, 1514–1531.
15. Lian, X., Bao, X., Al-Ahmad, A., Liu, J., Wu, Y., Dong, W., Dunn, K.K., Shusta, E.V., and Palecek, S.P. (2014). Efficient differentiation of human pluripotent stem cells to endothelial progenitors via small-molecule activation of WNT signaling. Stem Cell Reports *3*, 804–816.
16. Nakatsu, M.N., Davis, J., and Hughes, C.C. (2007). Optimized fibrin gel bead assay for the study of angiogenesis. J. Vis. Exp., 186.
17. Brunetti-Pierri, N., Erez, A., Shchelochkov, O., Craigen, W., and Lee, B. (2009). Systemic hypertension in two patients with ASL deficiency: a result of nitric oxide deficiency? Mol. Genet. Metab. *98*, 195–197.
18. Fakler, C.R., Kaftan, H.A., and Nelin, L.D. (1995). Two cases suggesting a role for the L-arginine nitric oxide pathway in neonatal blood pressure regulation. Acta Paediatr. *84*, 460–462.
19. Baruteau, J., Jameson, E., Morris, A.A., Chakrapani, A., Santra, S., Vijay, S., Kocadag, H., Beesley, C.E., Grunewald, S., Murphy, E., et al. (2017). Expanding the phenotype in argininosuccinic aciduria: need for new therapies. J. Inherit. Metab. Dis. *40*, 357–368.
20. Premkumar, M.H., Sule, G., Nagamani, S.C., Chakkalakal, S., Nordin, A., Jain, M., Ruan, M.Z., Bertin, T., Dawson, B., Zhang, J., et al. (2014). Argininosuccinate lyase in enterocytes protects from development of necrotizing enterocolitis. Am. J. Physiol. Gastrointest. Liver Physiol. *307*, G347–G354.
21. Stuehr, D., Pou, S., and Rosen, G.M. (2001). Oxygen reduction by nitric-oxide synthases. J. Biol. Chem. *276*, 14533–14536.
22. Yu, J., Vodyanik, M.A., Smuga-Otto, K., Antosiewicz-Bourget, J., Frane, J.L., Tian, S., Nie, J., Jonsdottir, G.A., Ruotti, V., Stewart, R., et al. (2007). Induced pluripotent stem cell lines derived from human somatic cells. Science *318*, 1917–1920.
23. Hitomi, T., Habu, T., Kobayashi, H., Okuda, H., Harada, K.H., Osafune, K., Taura, D., Sone, M., Asaka, I., Ameku, T., et al. (2013). Downregulation of Securin by the variant RNF213 R4810K (rs112735431, G>A) reduces angiogenic activity of induced pluripotent stem cell-derived vascular endothelial cells from moyamoya patients. Biochem. Biophys. Res. Commun. *438*, 13–19.
24. Theodoris, C.V., Li, M., White, M.P., Liu, L., He, D., Pollard, K.S., Bruneau, B.G., and Srivastava, D. (2015). Human disease modeling reveals integrated transcriptional and epigenetic

mechanisms of NOTCH1 haploinsufficiency. Cell *160*, 1072–1086.
25. Gu, M., Shao, N.Y., Sa, S., Li, D., Termglinchan, V., Ameen, M., Karakikes, I., Sosa, G., Grubert, F., Lee, J., et al. (2017). Patient-specific iPSC-derived endothelial cells uncover pathways that protect against pulmonary hypertension in BMPR2 mutation carriers. Cell Stem Cell *20*, 490–504.e5.
26. Lim, R.G., Quan, C., Reyes-Ortiz, A.M., Lutz, S.E., Kedaigle, A.J., Gipson, T.A., Wu, J., Vatine, G.D., Stocksdale, J., Casale, M.S., et al. (2017). Huntington's disease iPSC-derived brain microvascular endothelial cells reveal WNT-mediated angiogenic and blood-brain barrier deficits. Cell Rep. *19*, 1365–1377.
27. Fusaki, N., Ban, H., Nishiyama, A., Saeki, K., and Hasegawa, M. (2009). Efficient induction of transgene-free human pluripotent stem cells using a vector based on Sendai virus, an RNA virus that does not integrate into the host genome. Proc. Jpn. Acad., Ser. B, Phys. Biol. Sci. *85*, 348–362.
28. Huang, N.F., Fleissner, F., Sun, J., and Cooke, J.P. (2010). Role of nitric oxide signaling in endothelial differentiation of embryonic stem cells. Stem Cells Dev. *19*, 1617–1626.
29. Nie, Y., Zhang, K., Zhang, S., Wang, D., Han, Z., Che, Y., Kong, D., Zhao, Q., Han, Z., He, Z.X., et al. (2017). Nitric oxide releasing hydrogel promotes endothelial differentiation of mouse embryonic stem cells. Acta Biomater. *63*, 190–199.
30. Lund, A.K., Agbor, L.N., Zhang, N., Baker, A., Zhao, H., Fink, G.D., Kanagy, N.L., and Walker, M.K. (2008). Loss of the aryl hydrocarbon receptor induces hypoxemia, endothelin-1, and systemic hypertension at modest altitude. Hypertension *51*, 803–809.
31. Goodwin, J.E., Zhang, J., Gonzalez, D., Albinsson, S., and Geller, D.S. (2011). Knockout of the vascular endothelial glucocorticoid receptor abrogates dexamethasone-induced hypertension. J. Hypertens. *29*, 1347–1356.
32. Goodwin, J.E., and Geller, D.S. (2012). Glucocorticoid-induced hypertension. Pediatr. Nephrol. *27*, 1059–1066.
33. Bir, S.C., Xiong, Y., Kevil, C.G., and Luo, J. (2012). Emerging role of PKA/eNOS pathway in therapeutic angiogenesis for ischaemic tissue diseases. Cardiovasc. Res. *95*, 7–18.
34. Bussolino, F., Di Renzo, M.F., Ziche, M., Bocchietto, E., Olivero, M., Naldini, L., Gaudino, G., Tamagnone, L., Coffer, A., and Comoglio, P.M. (1992). Hepatocyte growth factor is a potent angiogenic factor which stimulates endothelial cell motility and growth. J. Cell Biol. *119*, 629–641.
35. Huang, J., and Kontos, C.D. (2002). PTEN modulates vascular endothelial growth factor-mediated signaling and angiogenic effects. J. Biol. Chem. *277*, 10760–10766.
36. Goumans, M.J., Liu, Z., and ten Dijke, P. (2009). TGF-beta signaling in vascular biology and dysfunction. Cell Res. *19*, 116–127.
37. Nakashima, H., Suzuki, H., Ohtsu, H., Chao, J.Y., Utsunomiya, H., Frank, G.D., and Eguchi, S. (2006). Angiotensin II regulates vascular and endothelial dysfunction: recent topics of Angiotensin II type-1 receptor signaling in the vasculature. Curr. Vasc. Pharmacol. *4*, 67–78.
38. Birdsey, G.M., Shah, A.V., Dufton, N., Reynolds, L.E., Osuna Almagro, L., Yang, Y., Aspalter, I.M., Khan, S.T., Mason, J.C., Dejana, E., et al. (2015). The endothelial transcription factor ERG promotes vascular stability and growth through Wnt/β-catenin signaling. Dev. Cell *32*, 82–96.
39. Rodrigo, R., Prat, H., Passalacqua, W., Araya, J., Guichard, C., and Bächler, J.P. (2007). Relationship between oxidative stress and essential hypertension. Hypertens. Res. *30*, 1159–1167.
40. Brito, R., Castillo, G., Gonzalez, J., Valls, N., and Rodrigo, R. (2015). Oxidative stress in hypertension: mechanisms and therapeutic opportunities. Exp. Clin. Endocrinol. Diabetes *123*, 325–335.
41. Noon, J.P., Walker, B.R., Webb, D.J., Shore, A.C., Holton, D.W., Edwards, H.V., and Watt, G.C. (1997). Impaired microvascular dilatation and capillary rarefaction in young adults with a predisposition to high blood pressure. J. Clin. Invest. *99*, 1873–1879.
42. Humar, R., Zimmerli, L., and Battegay, E. (2009). Angiogenesis and hypertension: an update. J. Hum. Hypertens. *23*, 773–782.
43. Agbor, L.N., Elased, K.M., and Walker, M.K. (2011). Endothelial cell-specific aryl hydrocarbon receptor knockout mice exhibit hypotension mediated, in part, by an attenuated angiotensin II responsiveness. Biochem. Pharmacol. *82*, 514–523.
44. Batshaw, M.L., Tuchman, M., Summar, M., Seminara, J.; and Members of the Urea Cycle Disorders Consortium (2014). A longitudinal study of urea cycle disorders. Mol. Genet. Metab. *113*, 127–130.

**The American Journal of Human Genetics, Volume *103***

## Supplemental Data

# Argininosuccinate Lyase Deficiency Causes an Endothelial-Dependent Form of Hypertension

**Jordan Kho, Xiaoyu Tian, Wing-Tak Wong, Terry Bertin, Ming-Ming Jiang, Shan Chen, Zixue Jin, Oleg A. Shchelochkov, Lindsay C. Burrage, Anilkumar K. Reddy, Hong Jiang, Reem Abo-Zahrah, Shuangtao Ma, Ping Zhang, Karl-Dimiter Bissig, Jean J. Kim, Sridevi Devaraj, George G. Rodney, Ayelet Erez, Nathan S. Bryan, Sandesh C.S. Nagamani, and Brendan H. Lee**

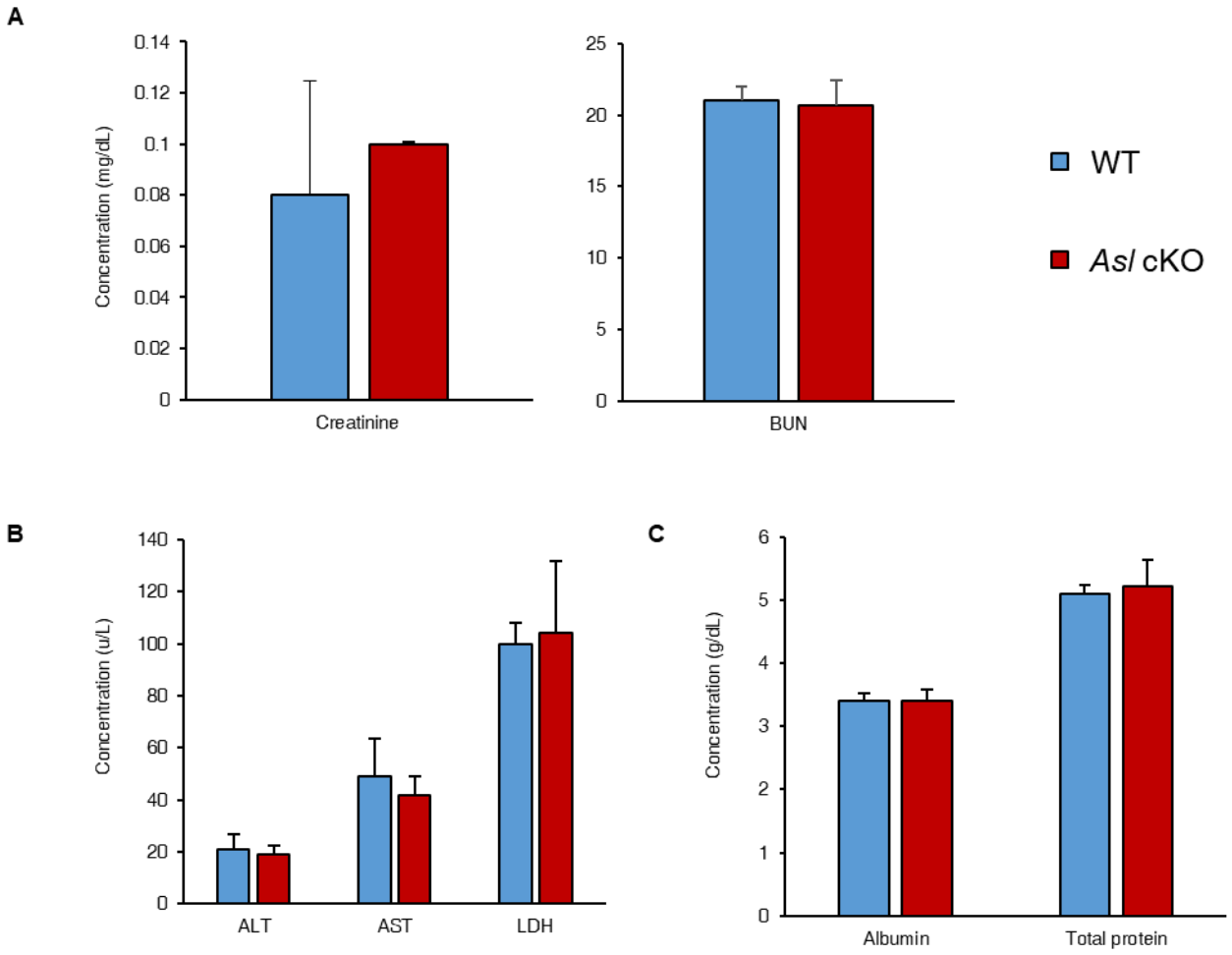


**Figure S1.** ***Asl*** **cKO mice display normal serum level of biomarkers for kidney and liver functions**

Serum level of (**A**) Creatinine, BUN, (**B**) ALT, AST, LDH, (**C**) albumin, and total protein in *Asl* cKO mice as compared to their wild-type littermates (n = 5, age = 12 weeks). Bar graphs represent mean values while error bars represent the standard deviation. Student's t-test.

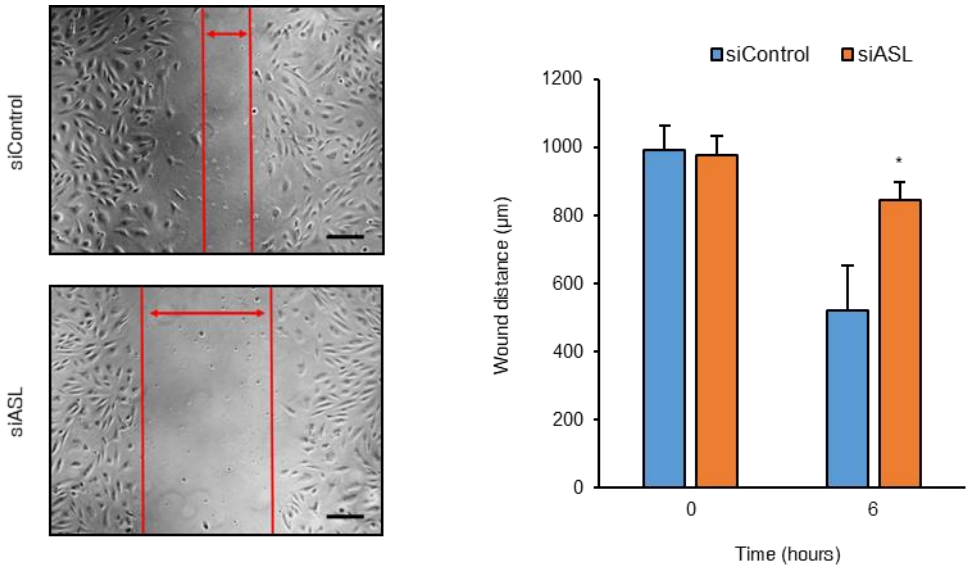


**Figure S2. Loss of ASL in HAECs impairs cell migration**
Wound healing assay performed on siASL-transfected HAECs. Wound distance was measured at t=0 h and t=8 h after wounding (n = 3). Scale bar, 200 µm. Bar graphs represent mean values while error bars represent the standard deviation. *P<0.05. Student's t-test.

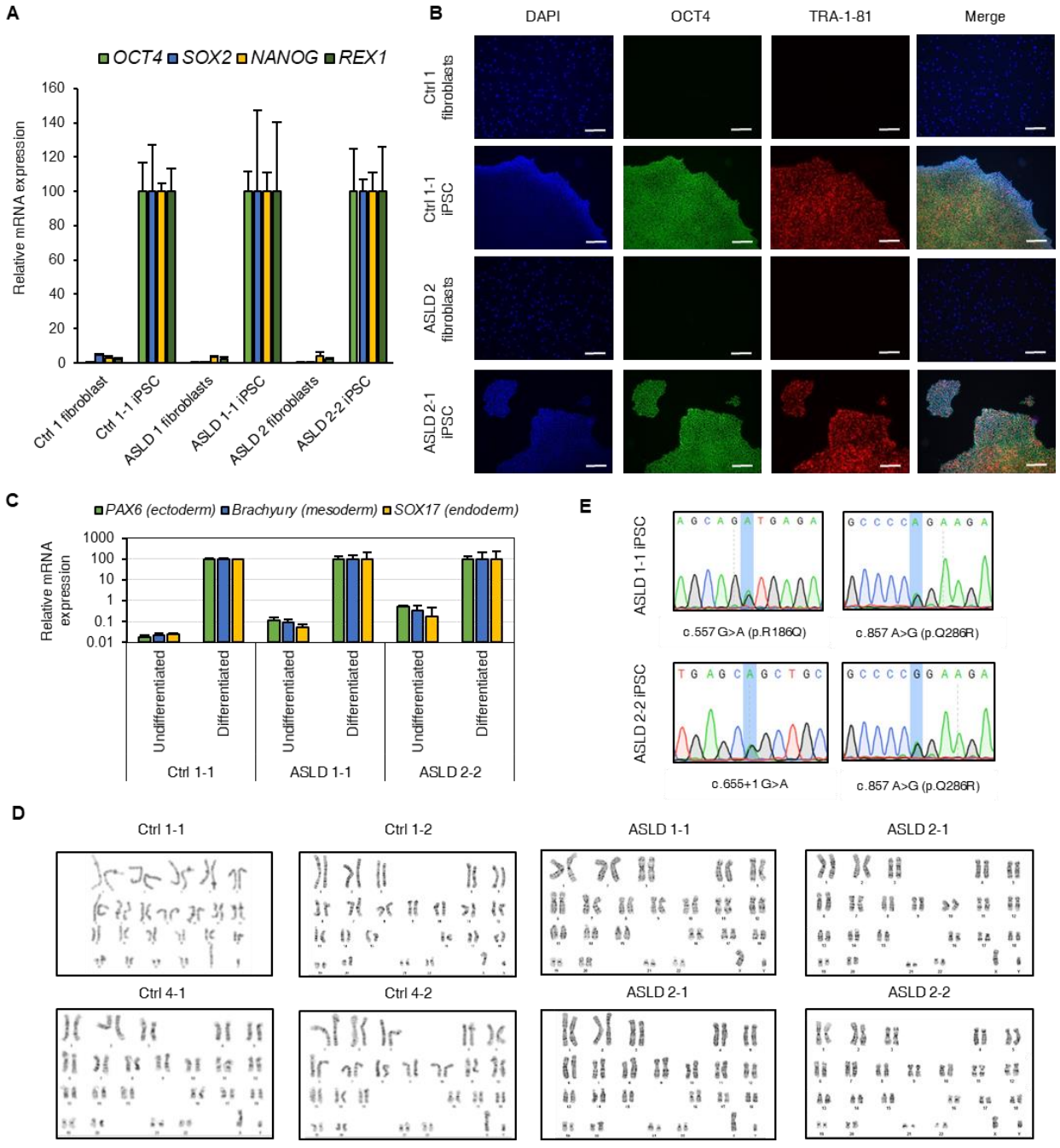


**Figure S3. Characterization of iPSC lines from healthy individuals and subjects with ASLD**
(**A**) Relative mRNA expression of pluripotency markers in representative fibroblasts and iPSC lines (n = 3). (**B**) Immunocytochemistry of pluripotency markers in representative control and ASLD iPSC lines. Scale bar, 200 µm. (**C**) Relative mRNA expression of endodermal, mesodermal, and ectodermal markers in representative iPSC lines upon differentiation into each respective germ layer (n = 3). (**D**) Karyotypes of control and ASLD iPSC lines. (**E**) Sanger sequencing showing that the ASLD iPSC lines continue to harbor the mutations present in the patient fibroblasts (GenBank: NM_001024943.1). Error bars represent the standard deviation.

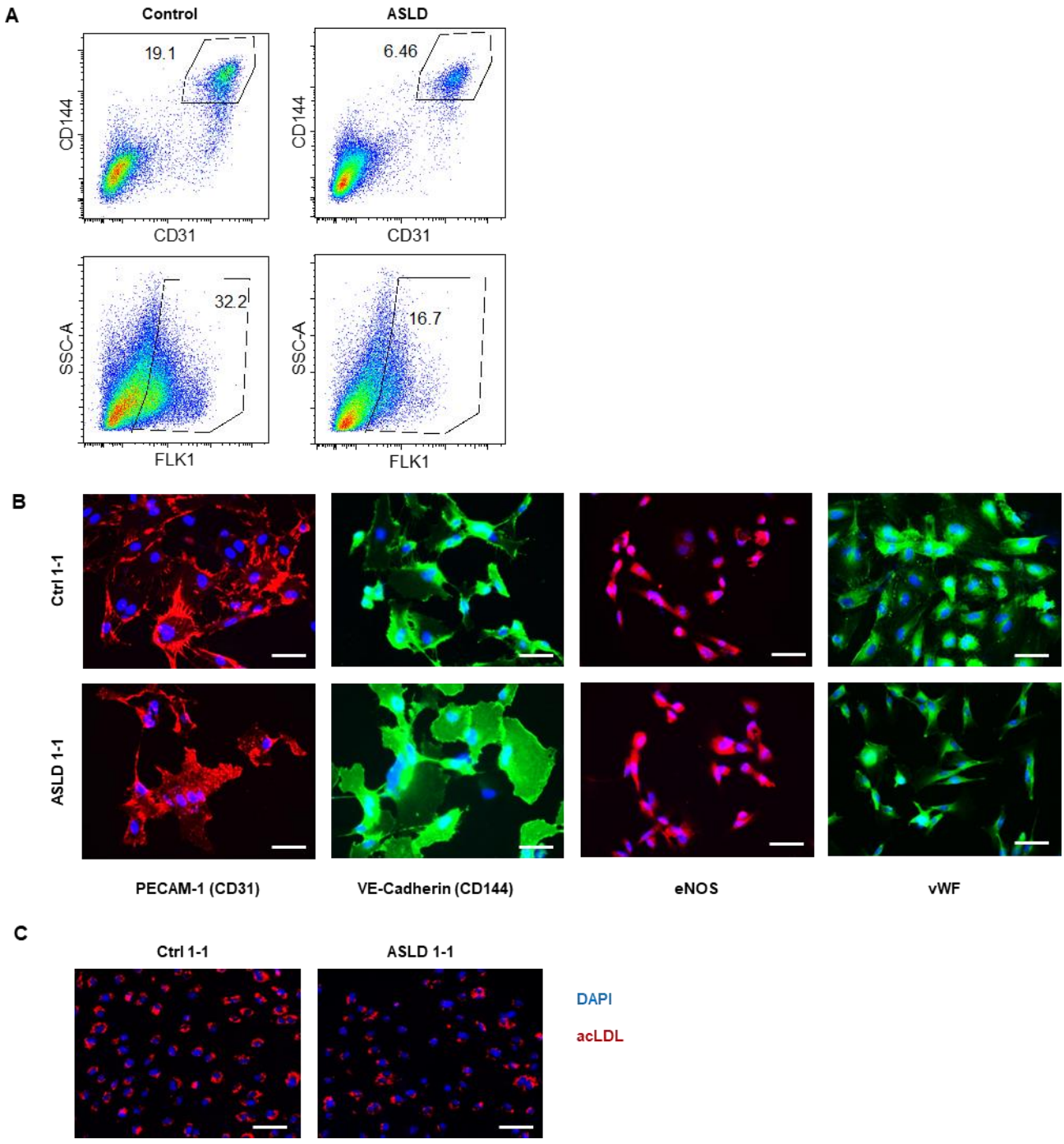


**Figure S4. Generation of hiPSC-derived endothelial cells**
(**A**) Representative FACS data obtained by sorting of CD31+/CD144+ and Flk1+ cells from differentiated control and ASLD iPSC. (**B**) Immunocytochemistry of endothelial markers in representative control and ASLD iPSC-ECs. Scale bar, 50 µm. (**C**) Representative images of uptake of acetylated LDL (acLDL) by iPSC-ECs. Scale bar, 100 µm.

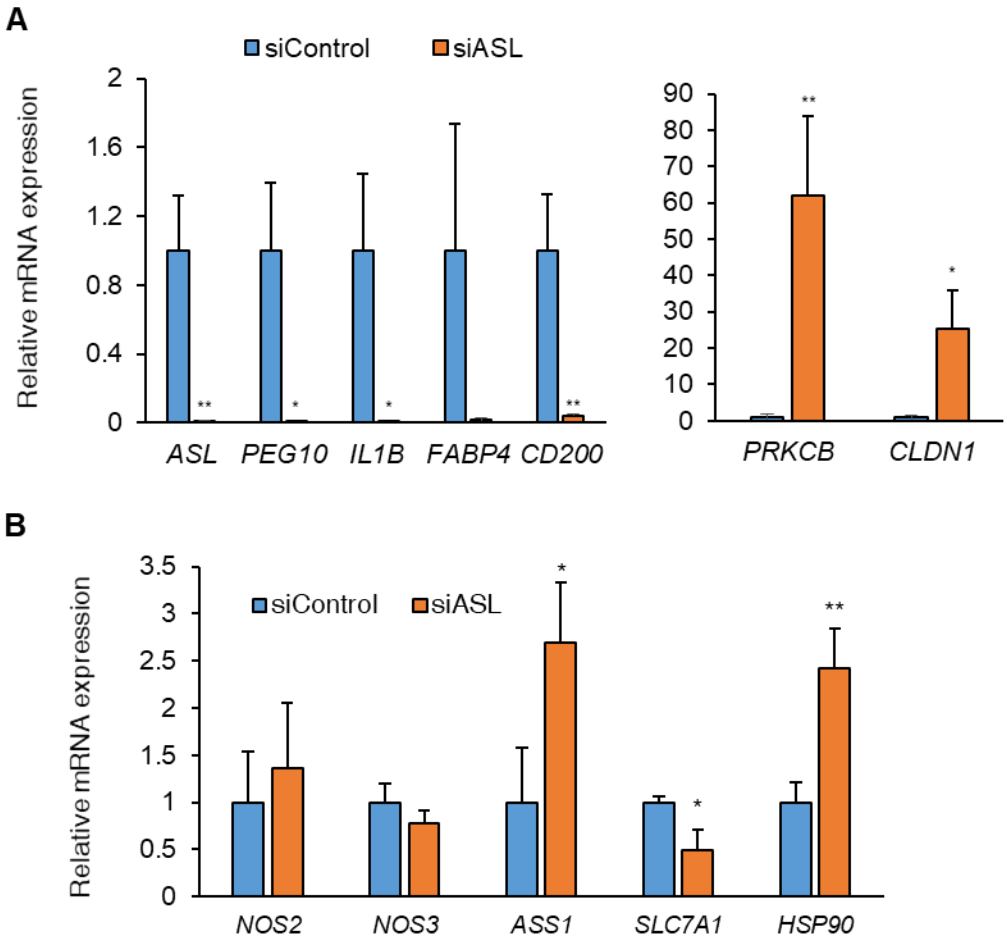


**Figure S5. qRT-PCR confirmation of RNA-Sequencing gene expression patterns in ASL-deficient HAECs**

The mRNA expression level of (**A**) top dysregulated and (**B**) NO synthesis complex genes in siASL-transfected HAECs were quantified by qRT–PCR (n = 3 biological replicates of siControl and siASL). *NOS1* expression in HAECs was undetectable by qRT-PCR. Bar graphs represent mean values while error bars represent the standard deviation. *P<0.05 and **P<0.01. Student's t-test.

.

| Subject | Age (years) | Sex | Height (cm) | Weight (kg) | BMI |
|---|---|---|---|---|---|
| 100006 | 13.8 | M | 169 | 63 | 22.06 |
| 101893 | 13.0 | M | 141 | 43 | 21.90 |
| 100551 | 4.5 | M | 98 | 18 | 18.74 |
| 101880 | 10.1 | F | 130 | 29 | 17.16 |
| 102635 | 9.1 | F | 131 | 27 | 15.73 |
| 102747 | 11.2 | F | 127 | 23 | 14.26 |
| 104591 | 13.4 | F | 155 | 38 | 15.82 |
| 106088 | 13.8 | F | 160 | 51 | 19.92 |

**Table S1. Demographic characteristics of individuals with ASLD enrolled in the trial NCT00345605**

| iPSC line | Sex | Diagnosis | Age at biopsy (years) | Pathogenic variants in ASL | Source of cells | Method of iPSC derivation | Reprogramming factors | Notes |
|---|---|---|---|---|---|---|---|---|
| Ctrl1-1 | Male | Healthy control | 22 | N/A | Skin fibroblasts | Sendai virus | OCT4, SOX2, KLF4, c-MYC | Provided by BCM-Human Stem Cell Core (HSCC-003iPS) |
| Ctrl1-2 | | | | | | | | |
| Ctrl 2 | Male | Healthy control | 61 | N/A | Skin fibroblasts | Gamma-retrovirus | OCT4, SOX2, KLF4, c-MYC | N/A |
| Ctrl 3 | Male | Healthy control | N/A | N/A | Cord blood cells | Episomal vector | OCT4, SOX2, KLF4, c-MYC | Purchased from Applied StemCell |
| Ctrl 4-1 | Male | Healthy control | 16 | N/A | Skin fibroblasts | Sendai virus | OCT4, SOX2, KLF4, c-MYC | Provided by BCM-Human Stem Cell Core (HSCC-022iPS) |
| Ctrl 4-2 | | | | | | | | |
| ASLD 1-1 | Male | ASLD | 16 | c.557 G>A (p.R186Q)<br>c.857 A>G (p.Q286R) | Skin fibroblasts | Sendai virus | OCT4, SOX2, KLF4, c-MYC | N/A |
| ASLD 1-2 | | | | | | | | |
| ASLD 2-1 | Male | ASLD | 10 | c.655+1 G>A<br>c.857 A>G (p.Q286R) | Skin fibroblasts | Sendai virus | OCT4, SOX2, KLF4, c-MYC | N/A |
| ASLD 2-2 | | | | | | | | |

**Table S2. List of iPSC lines and methods of derivation**

| | Gene | | FPKM | | log2(fold change) |
|---|---|---|---|---|---|
| | | | siControl | siASL | |
| Top downregulated genes | SNORD116-4 | small nucleolar RNA, C/D box 116-4 | 31.750 | 0 | |
| | LINC01173 | long intergenic non-protein coding RNA 1173 | 0.773 | 0 | |
| | PEG10 | Paternally expressed 10 | 22.079 | 0.171 | -7.011 |
| | IL1B | Interleukin-1 beta | 22.901 | 0.533 | -5.425 |
| | CD200 | OX-2 membrane glycoprotein | 14.678 | 0.463 | -4.988 |
| | ASL | Argininosuccinate lyase | 15.056 | 0.520 | -4.856 |
| | FABP4 | Fatty acid-binding protein, adipocyte | 16.898 | 0.610 | -4.793 |
| | GNG2 | Guanine nucleotide-binding protein G(I)/G(S)/G(O) subunit gamma-2 | 1.261 | 0.049 | -4.687 |
| | CEND1 | Cell cycle exit and neuronal differentiation protein 1 | 1.934 | 0.089 | -4.448 |
| | CORO1A | Coronin-1A | 3.524 | 0.173 | -4.347 |
| Top upregulated genes | KIAA1644 | Uncharacterized protein KIAA1644 | 0.059 | 1.641 | 4.794 |
| | PRKCB | Protein kinase C beta type | 0.017 | 0.433 | 4.633 |
| | CLDN1 | Claudin-1 | 0.222 | 5.105 | 4.522 |
| | GHR | Growth hormone receptor | 0.034 | 0.485 | 3.839 |
| | PLSCR4 | Phospholipid scramblase 4 | 3.593 | 46.199 | 3.685 |
| | NTSR1 | Neurotensin receptor type 1 | 0.101 | 1.302 | 3.683 |
| | P2RY6 | P2Y purinoceptor 6 | 0.174 | 2.185 | 3.648 |
| | SRRM3 | Serine/arginine repetitive matrix protein 3 | 0.059 | 0.736 | 3.631 |
| | SCN1B | Sodium channel subunit beta-1 | 2.373 | 27.276 | 3.523 |
| | TGFB2 | Transforming growth factor beta-2 | 0.246 | 2.778 | 3.500 |

**Table S3. List of top dysregulated genes in ASL-deficient HAECs**

| Gene | | FPKM | | log2(fold change) | Significant |
|---|---|---|---|---|---|
| | | siControl | siASL | | |
| NOS1 (nNOS) | Nitric oxide synthase 1 | 0.001 | 0.003 | 1.221 | no |
| NOS2 (iNOS) | Nitric oxide synthase 2 | 0 | 0.007 | | no |
| NOS3 (eNOS) | Nitric oxide synthase 3 | 33.186 | 33.496 | 0.013 | no |
| ASS1 | Argininosuccinate synthase | 0.315 | 1.701 | 2.430 | yes |
| SLC7A1 | High affinity cationic amino acid transporter 1 | 20.571 | 7.026 | -1.550 | yes |
| HSP90AA1 | Heat shock protein HSP 90-alpha | 369.379 | 437.263 | 0.243 | yes |

**Table S4. Effects of ASL deficiency on expression of components of NO synthesis complex in HAECs**